Tip-Enhanced Raman Imaging of Plasmon-Driven Dimerization of 4-Bromothiophenol on Nickel-Decorated Gold Nanoplates Bimetallic Nanostructures

Swati Patil[a], and Dmitry Kurouski*[a,b]

[a]Department of Biochemistry and Biophysics, Texas A&M University, College Station, Texas 77843, United States

[b]Department of Biomedical Engineering, Texas A&M University, College Station, Texas, 77843, United States

Corresponding Author

*Dmitry Kurouski

[a]Department of Biochemistry and Biophysics, Texas A&M University, College Station, Texas 77843, United States

[b]Department of Biomedical Engineering, Texas A&M University, College Station, Texas, 77843, United States

orcid.org/0000-0002-6040-4213; Email: dkurouski@tamu.edu

KEYWORDS: Gold-nickel nanostructures, plasmonic, photocatalysis, TERS imaging.

Supporting information

Experimental

Chemicals: Gold (III) chloride trihydrate ($HAuCl4 \cdot 3H_2O$, 99.9%), nickel chloride ($NiCl_2$) hexadecyltrimethylammonium bromide (CTAB, 99%), sodium hydroxide (NaOH, 98%), poly (vinyl pyrrolidone) (PVP, average mol wt 29000), polyvinylpyrrolidone (PVP, and 4-nitrobenzenethiol (4-NBT, 80%), Hydrazine hydrate (80% solution in water) were purchased from Sigma-Aldrich (St. Louis, MO). Sodium citrate dihydrate (Na-Cit, 99%) was purchased from Fisher scientific (Waltham, MA). Ethanol was purchased from Decon Labs (King of Prussia, PA). All chemicals were used as received without purification.

Synthesis of Au Nanoparticles (NPs)

Gold nanoplates were synthesized as follows by the Turkevich method.43 Initially, Au stock solution was prepared by dissolving 1 mM HAuCl4 in 125 mL double distilled water (DDW) with heating (80°C) and stirring for 30 minutes. Furthermore, the yellowish stock solution was distributed evenly in five beakers with 25 mL. Furthermore, the molar ratio of the repeating unit of PVP to HAuCl4 stock solution of 0.1 mM, 1 mM, 2 mM, 5 mM, and 8 mM PVP were added in sequence, followed by good mechanical stirring and heating. The reaction mixture turned colorless initially. To ensure complete reduction, 1.87 mL of Na-cit (7 mM) aqueous solution was quickly added to each of the five solutions while heating for 1 hour. The reduction of Au3+ to Au+ by Na-cit is caused by the loss of solution color. The color of the final solution changes from colorless to red, then purple blue in a fraction of a second due to the formation of nanoplates. Meanwhile, increasing PVP concentration causes a slowing of nanoplate nucleation and growth. The reducing agent has a significant impact on the shape and size of the nanoplates. Small nanoplates are mostly spherical and triangular, whereas larger plates are cubic, pentagonal, and hexagonal. The size of the nanoplate appears to be influenced by the relative number of nuclei formed by the reduction by Na-cit in comparison to the remaining gold ions which weren't completely reduced to Au0: the less the initial nuclei, the larger the resulting nanoplates. If plates are bigger the color of the solution changed gradually. The number of nuclei in solution decreases with increasing PVP concentration, as indicated by the reaction rate. Furthermore, completing nucleation and growth, all solutions were allowed to cool at room temperature. Furthermore, the settled product was collected by centrifuging it several times to remove the binders. Finally, the various nanostructures were obtained such as spheres (0.1

mM PVP), tringle (1 mM PVP), cubes (2 mM PVP), pentagonal (5 mM PVP), and hexagonal (8 mM PVP). The obtained triangular and hexagonal nanoplates were then used to decorate Ni nanoparticles.

Synthesis of Ni@AuNPs

NiNPs were synthesized in an aqueous solution. We selected two shapes (trigonal and hexagonal) of Au NPs for the decoration of Ni NPs. We followed two steps in the synthesis of Ni@AuNPs. In the first step, 25 mL of aqueous solution A was prepared by dissolving 10 mM CTAB and 5 mM NiCl2 at room temperature while stirring. After stirring for 20 minutes, 10 mL of trigonal or hexagonal-shaped Au NPs were added to solution A. In the second step, 10 ml of aqueous solution B was made separately by adding 20 mM NaOH and then 25 mM hydrazine while mechanically stirring. A resultant solution was obtained by mixing solution B dropwise in solution A. The final solution was kept at room temperature for 2 hours in a capped bottle, and Ni nanoparticles were decorated on the Au formed in the solution. To remove the surfactants and other impurities from the Ni@AuNPs, the precipitated solution was centrifuged at 10000 rpm for 15 minutes and washed several times with ethanol and DDW.

Deposition of 4-NBP on Ni@AuNPs

The as-synthesized Ni@AuNPs were first deposited on a precleaned Si wafer. Typically, 10 μL of ethanolic Ni@AuNPs solution was drop-casted on a 0.5 cm^2 Si wafer and dried it at room temperature. It was then rinsed with ethanol to remove the excess unbounded NPs and dried with N_2-air. In the subsequent step, a monolayer of 4-NBT was created by drop-casting 10 μL of ethanolic 4-NBT solution onto a previously prepared on Ni@AuNPs on Si wafer. It was also rinsed with ethanol several times to remove any unbounded 4-NBT molecules before being dried with N_2-air.

TER Probe Fabrication

AFM tips with resonance frequency: 50-80 kHz, amplitude: 20 nm, and force constant: 2.7 N/m were purchased from Appnano (Mountain View, CA). TERS images with low and high magnification are scanned at 125 nm/s and 20 nm/s, respectively. AFM tips further modified with metal deposition. For Au (Kurt J. Lesker, Efferson Hills, PA) deposition, AFM tips were placed in a thermal evaporator (MBrown, Stratham, NH) and metal deposition was conducted at $\sim 1\times10^{-6}$ mbar with deposition rate of 0.1 A/s. The tip surface temperature was 50 °C, to obtain a final thickness of 70 nm.

AFM-TERS Imaging

Images from atomic force microscopy (AFM) and tip-enhanced Raman (TER) were acquired using the AIST-NT-HORIBA system, which is fitted with a 633 nm continuous wavelength (CW) laser. Using a 100× Mitutoyo microscope objective, laser light was directed at the sample in a side-illumination geometry. The same objective was used to collect scattered electromagnetic radiation and direct it into a HORIBA iHR550 spectrograph equipped with a Synapse EM-CCD camera (HORIBA, Edison, NJ).

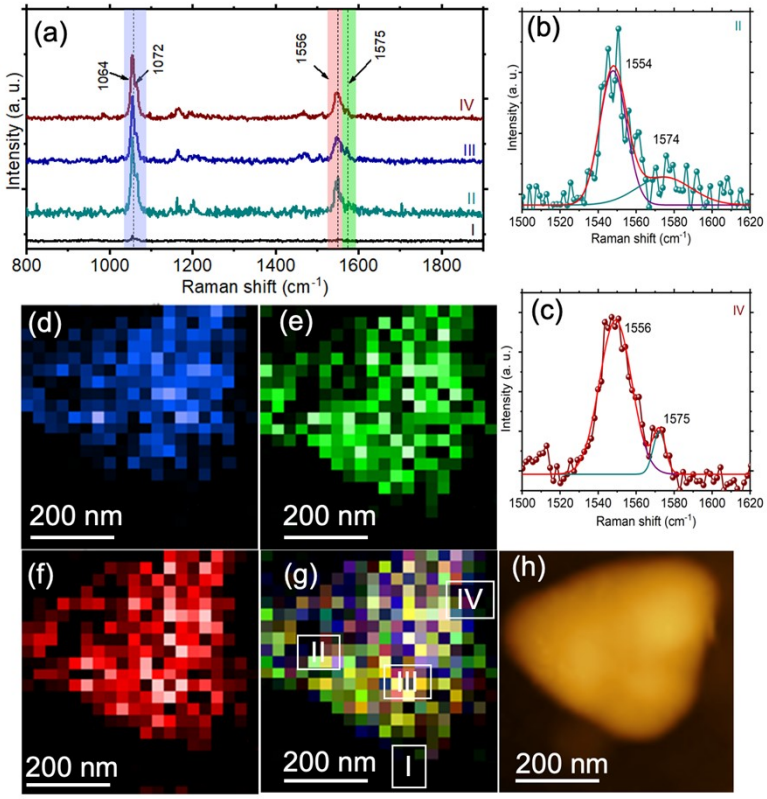

Figure S1. Plasmon-driven dehalogenation of 4-BTP on AuNPs. **(a)** Selected TER spectra acquired from AuNP at different areas outlined in **(g)** on Si wafer which confirm the presence of intact 4-BTP (1064 cm^{-1} (νC-Br), 1072 cm^{-1} (νCS), 1556 cm^{-1} (νC-$C_{(ring)}$)), and 4-BTP with a formation of TP (1575 cm^{-1} (νC-$C_{(ring)}$) on AuNPs. The best fitted spectrum for the outlined (II) and (IV) are shown in **(b)** and **(c)**, respectively. TER images of **(d)** 4-BTP (1064 and 1072 cm^{-1}), **(e)** 4-BTP (1556 cm^{-1}) and **(f)** TP (1575 cm^{-1}). The overlapped images of **(d), (e)**, and **(f)** in **(g)** and the corresponding AFM image of the AuNPs **(h)**.

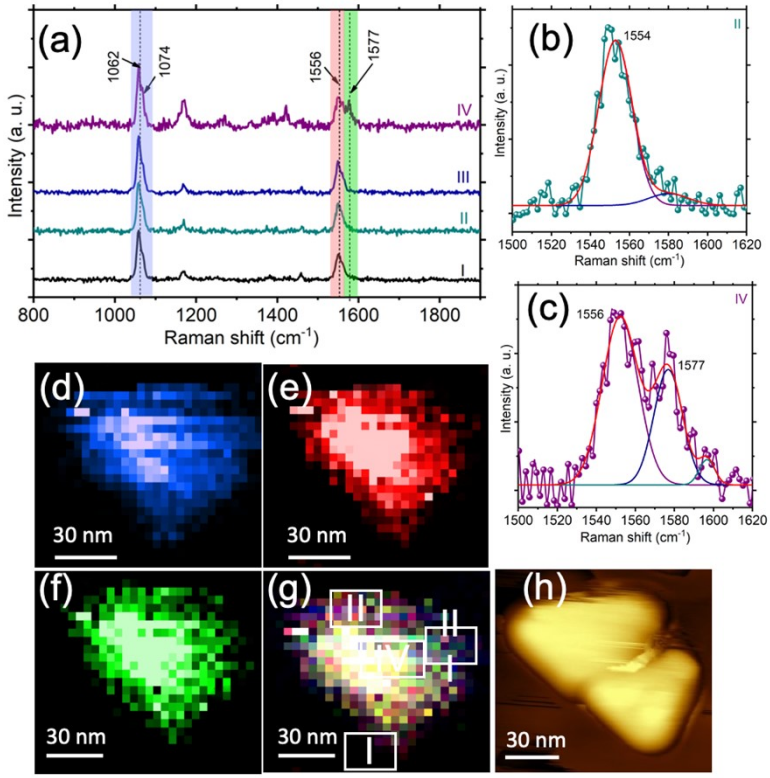

Figure S2. Plasmon-driven dehalogenation of 4-BTP on AuNPs. **(a)** Selected TERS spectra acquired from Si substrate (I) and AuNPs (II-IV) which confirm the presence of intact 4-BTP **(b)** and a mixture of 4-BTP and TP **(c)** on AuNPs. **(d-g)** TERS images of distribution of **(d)** 4-BTP (1064 cm^{-1} (vC-Br), 1074 cm^{-1} (vCS) and **(e)** 1556 cm^{-1} (vC-$C_{(ring)}$) and **(f)** TP (1577 cm^{-1} (vC-$C_{(ring)}$)), as well as **(g)** the overlaid (1064 cm^{-1}, 1556 cm^{-1}, and 1577 cm^{-1}) together with **(h)** the corresponding AFM image of the nanoplate.

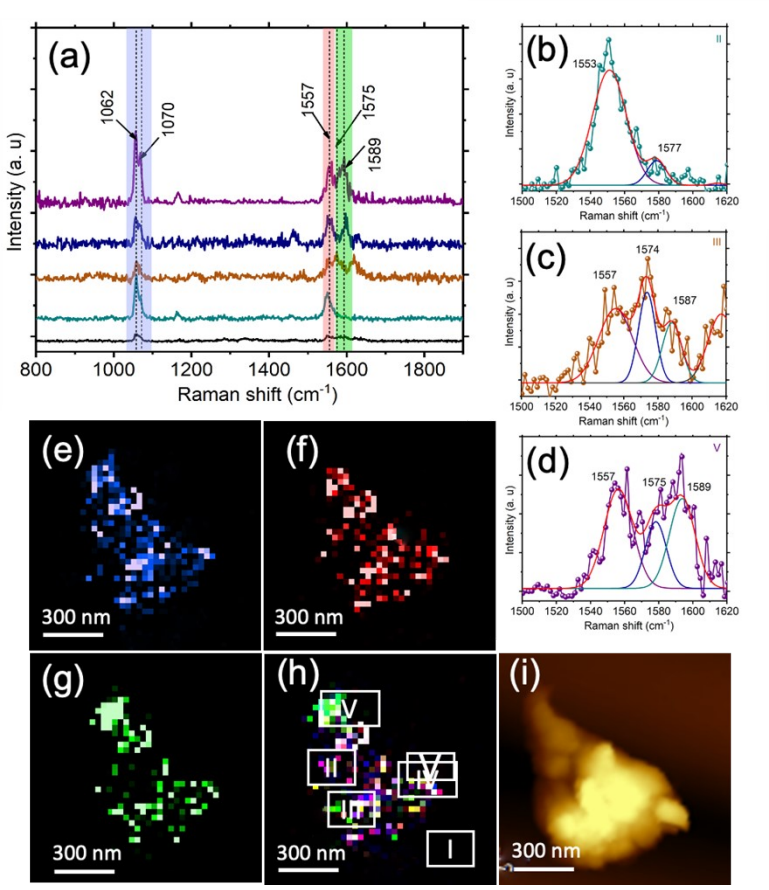

Figure S3. Plasmon-driven formation of BPDT and TP on Ni@AuNPs. **(a)** Selected TERS spectra acquired from Si substrate (I) and Ni@AuNPs (II-IV) which confirm the presence of intact 4-BTP **(b)** and a mixture of 4-BTP, TP and BPDT **(c-d)** on Ni@AuNPs. **(d-g)** TERS images of distribution of **(e)** 4-BTP (1062 cm^{-1} (vC-Br), 1077 cm^{-1} (vCS) and 1557 cm^{-1} (vC-$C_{(ring)}$), **(f)** TP (1575 cm^{-1} (vC-$C_{(ring)}$)), and **(g)** BPDT (1589 cm^{-1}) as well as **(h)** the overlaid (1062 cm^{-1}, 1577 cm^{-1}, and 1589 cm^{-1}) together with **(h)** the corresponding AFM image of the nanoplate.

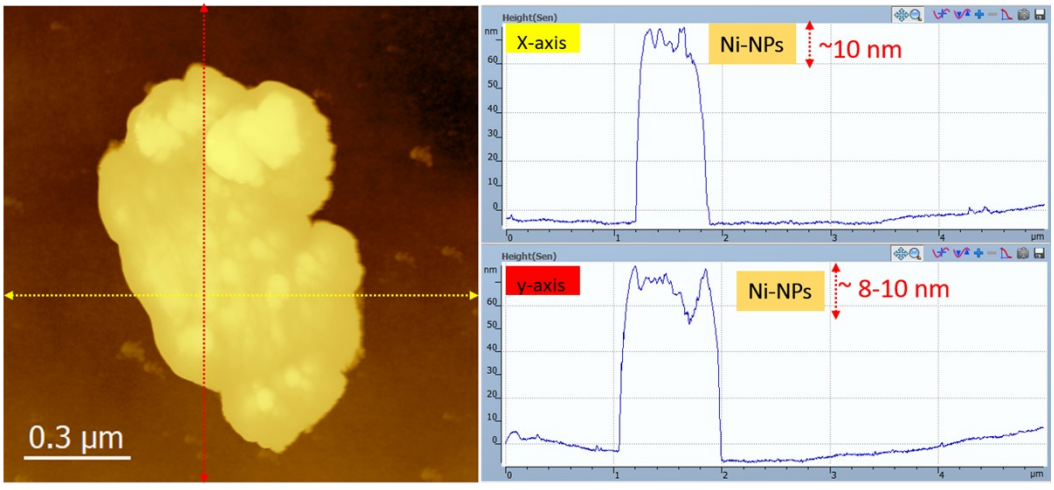

Figure S4. AFM image of the Ni@AuNPs and corresponding height profiles.

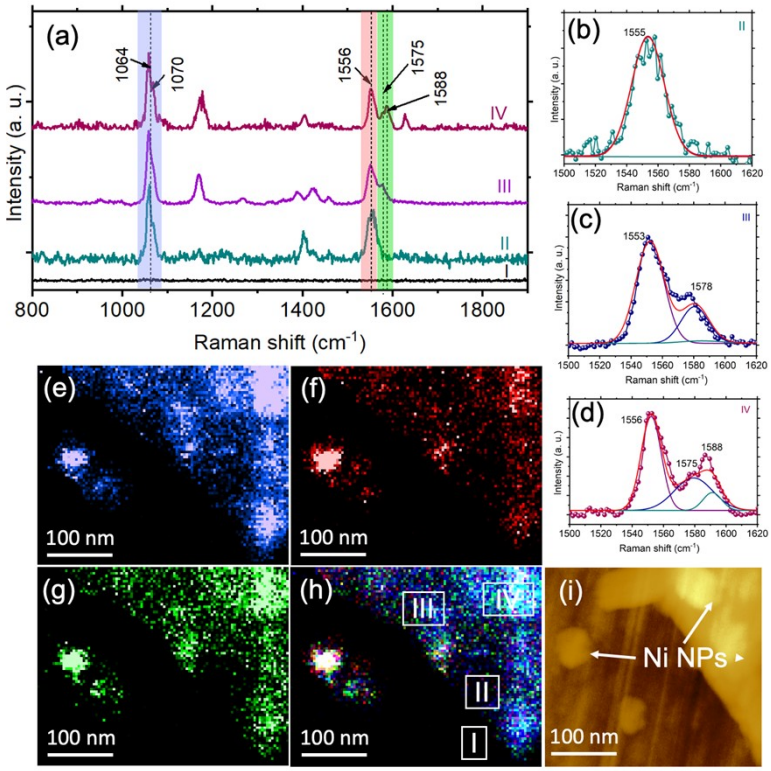

Figure S5. TERS monitoring the plasmon-driven formation of 4,4'-BPDT and TP on Ni@AuNPs. Typical TER spectra acquired from the marked different positions in **(h)** and the corresponding AFM image **(i)**. The deconvoluted spectrum confirms that the catalytic reaction occurs at surface of Ni@AuNPs. TER extracted a spectrum containing intact 4-BTP **(b)**, doublet peaks for 4-BTP and TP (c) and triplet peaks for the 4-BTP, TP and 4,4'-BPDT **(d)** on Ni@AuNPs. TERS maps of **(e)** 4-BTP (1064 cm^{-1} (vC-Br) and 1070 cm^{-1} (vCS)) and **(f)** 4-BTP 1556 cm^{-1} (vC-$C_{(ring)}$), **(g)** TP (1575 cm^{-1} (vC-$C_{(ring)}$)), and 4,4'-BPDT (1588 cm^{-1}). **(h)** The overlapping TERS maps of **(e)**, **(f)** and **(g)**.

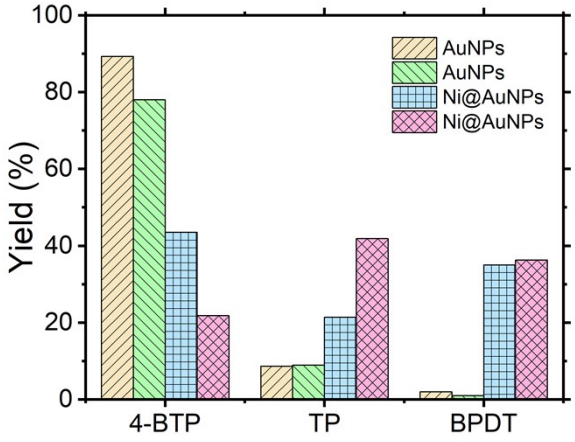

Figure S6. The bar diagram shows the plasmon-driven formation of TP and BPDT on Ni@AuNPs.